Reversible photoswitching of encapsulated azobenzenes in water

Dipak Samanta[a], Julius Gemen[a], Zonglin Chu[a], Yael Diskin-Posner[b], Linda J. W. Shimon[b], and Rafal Klajn[a,1]

[a]Department of Organic Chemistry, Weizmann Institute of Science, 76100 Rehovot, Israel; and [b]Department of Chemical Research Support, Weizmann Institute of Science, 76100 Rehovot, Israel

Edited by J. Fraser Stoddart, Northwestern University, Evanston, IL, and approved March 29, 2018 (received for review September 27, 2017)

Efficient molecular switching in confined spaces is critical for the successful development of artificial molecular machines. However, molecular switching events often entail large structural changes and therefore require conformational freedom, which is typically limited under confinement conditions. Here, we investigated the behavior of azobenzene—the key building block of light-controlled molecular machines—in a confined environment that is flexible and can adapt its shape to that of the bound guest. To this end, we encapsulated several structurally diverse azobenzenes within the cavity of a flexible, water-soluble coordination cage, and investigated their light-responsive behavior. Using UV/Vis absorption spectroscopy and a combination of NMR methods, we showed that each of the encapsulated azobenzenes exhibited distinct switching properties. An azobenzene forming a 1:1 host–guest inclusion complex could be efficiently photoisomerized in a reversible fashion. In contrast, successful switching in inclusion complexes incorporating two azobenzene guests was dependent on the availability of free cages in the system, and it involved reversible trafficking of azobenzene between the cages. In the absence of extra cages, photoswitching was either suppressed or it involved expulsion of azobenzene from the cage and consequently its precipitation from the solution. This finding was utilized to develop an information storage medium in which messages could be written and erased in a reversible fashion using light.

azobenzene | coordination cages | confinement | photochromism

Light-powered (1–3) and chemically fueled (4–7) artificial molecular machines have long been recognized as the key building blocks of the functional materials of the future (8–10). These unique molecules have traditionally been synthesized and studied in solution, where they have been successfully used to induce conformational chemical changes in bound guest molecules (1) or to synthesize other, smaller molecules (11, 12), among other applications (5). However, it has become increasingly evident that to fully explore and utilize their potential, it is necessary to confine molecular machines to the surfaces of larger objects (13, 14), such as inorganic nanoparticles (15, 16). Successful operation of surface-immobilized molecular machines has enabled additional attractive applications in, for example, the controlled release of molecular cargo (17), guiding the motion of liquid droplets (18), or even physical manipulation of macroscopic metallic objects (19).

However, the molecular motion associated with the operation of these machines requires a certain degree of conformational freedom, which is often not available under confinement. For example, it has long been known that confining azobenzene—the molecule of choice for constructing light-driven molecular machines—within densely packed self-assembled monolayers (20) or in the cavities of rigid self-assembled cages (21) can render it nonswitchable. Similarly, *trans* → *cis* photoisomerization of azobenzene bound in the cavities of other structurally robust supramolecular (22, 23) or macrocyclic (24–26) hosts entailed its expulsion from these cavities. It therefore becomes clear that efficient switching of confined azobenzenes requires hosts that are sufficiently flexible to accommodate the large conformational change (27, 28) accompanying azobenzene's isomerization.

Although the majority of self-assembled hosts reported to date are rigid (29), increasing attention has recently been devoted to flexible ones (30–33). Herein, we considered water-soluble coordination cage **1** (Fig. 1*A*) (34) as a potential host for various azobenzene switches. We envisioned that some degree of rotational flexibility about the $C_{benzene}$–N bond might result in significant conformational flexibility of the cage. This flexibility could be the key for not only encapsulating a wide range of structurally diverse azobenzenes, but also for accommodating both (i.e., *trans* and *cis*) isomers of the same azobenzene, thereby enabling efficient photoisomerization of azobenzenes in aqueous media.

Results and Discussion

We initially worked with unsubstituted azobenzene **2** (Fig. 1*B*). Although **2** has a very low solubility in pure water, it readily dissolves in aqueous solutions of **1**, which then assume an intense yellow color and a pronounced absorption band at ∼325 nm characteristic of the $\pi \rightarrow \pi^*$ transition of *trans*-azobenzene. We took advantage of the high molar absorptivity to study the solubilization kinetics of **2** (and other azobenzenes; see below). In these experiments, we stirred solid **2** (used in excess) with an aqueous solution of **1** at a known concentration of the cage. The reaction was discontinued at different time intervals by removing undissolved **2** by ultracentrifugation and the resulting supernatant was characterized by UV/Vis absorption spectroscopy. We found that the spectra did not change after the initial ∼6 h (*SI Appendix*, Fig. S3). To ensure that the reaction was complete, **2** and other azobenzenes used in this study were incubated with the cage solution for 24 h.

Significance

Azobenzene can be efficiently and reversibly switched between two structurally different forms upon exposure to different wavelengths of light and, as such, it is the molecule of choice for constructing light-powered molecular machines. The studies described herein show that several structurally different azobenzenes can be encapsulated within the cavity of a flexible, water-soluble molecular cage. The confined space of the cage was found to have a profound effect on azobenzenes' switching behavior. This study advances our understanding of azobenzene isomerization in condensed phases. At the same time, it paves the way toward investigating other molecular switches under confinement conditions and developing novel artificial molecular machines.

Author contributions: D.S., J.G., and R.K. designed research; D.S. and J.G. performed research; Z.C., Y.D.-P., and L.J.W.S. contributed new reagents/analytic tools; D.S., J.G., Y.D.-P., and L.J.W.S. analyzed data; and R.K. wrote the paper with contributions from all authors.

The authors declare no conflict of interest.

This article is a PNAS Direct Submission.

Data deposition: The atomic coordinates have been deposited in the Cambridge Structural Database, Cambridge Crystallographic Data Centre (CSD reference nos. 1551435, 1569281, 1551438, and 1569282).

[1]To whom correspondence should be addressed. Email: rafal.klajn@weizmann.ac.il.

This article contains supporting information online at www.pnas.org/lookup/suppl/doi:10.1073/pnas.1712787115/-/DCSupplemental.

Published online May 1, 2018.

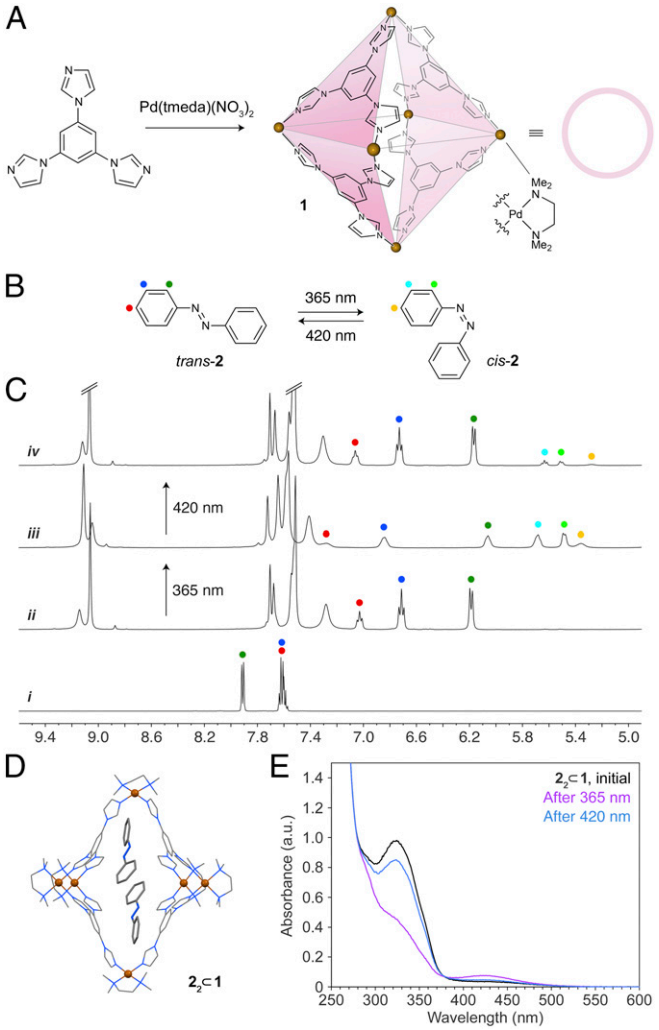

Fig. 1. Reversible photoswitching of unsubstituted azobenzene in water. (*A*) Synthesis of octahedral cage **1** from a triimidazole-based ligand and a *cis*-blocked Pd acceptor (34). (*B*) UV/blue light-induced isomerization of unsubstituted azobenzene **2**. (*C*) Changes in the NMR spectrum of *trans*-**2** (*i*) upon encapsulation within **1** (*ii*) and subsequent irradiation with UV light (*iii*) and blue light (*iv*). Spectrum *i* was recorded in $(CD_3)_2SO$ and spectra *ii*–*iv* in D_2O (400 MHz, 298 K). (*D*) X-ray crystal structure of (*trans*-**2**)$_2$ ⊂ **1** (see also *SI Appendix*, Fig. S15). Color codes for all X-ray structures: C, gray; N, blue; O, red; F, green; Pd, brown sphere. Hydrogens, counterions, and solvent molecules are not shown for clarity. (*E*) Changes in the UV/Vis absorption spectrum of (*trans*-**2**)$_2$ ⊂ **1** (black) following exposure to UV light (10 min, purple) and then to blue light (8 min, blue).

The amount of solubilized **2** depended on the concentration of **1** (which has a very high, >0.3 g/mL, solubility in water). Analysis by UV/Vis spectroscopy consistently showed that one equivalent of **1** enabled solubilization of ∼1.2 eq of **2**. To confirm this result, we analyzed the **1**·**2** complex by ^{1}H NMR spectroscopy and found that proton resonances associated with **2** were markedly (by 0.7–1.7 ppm) upfield-shifted (compare spectra *i* and *ii* in Fig. 1*C*), suggesting that **2** resided in the hydrophobic cavity of the cage. Integrating guest **2**'s and host **1**'s signals similarly afforded a ratio of ∼1.2 (*SI Appendix*, Fig. S5), which suggests that one molecule of **1** can accommodate more than one molecule of **2**. Indeed, X-ray diffraction on a single crystal obtained by slow water evaporation from a solution of **1** saturated with **2** revealed the presence of a 2:1 inclusion complex (i.e., $\mathbf{2}_2 \subset \mathbf{1}$; Fig. 1*D*). Within this complex, **2** interacts with **1** by π–π stacking interactions (*SI Appendix*); in addition, binding of **2** (and other azobenzenes, see below) within **1** is likely facilitated by hydrophobic interactions.

Interestingly, dissolution of crystalline $\mathbf{2}_2 \subset \mathbf{1}$ in water was followed by precipitation of free **2** within several minutes. The molar ratio of **2** to **1** in the resulting solution corresponds to ∼1.2 (*SI Appendix*, Fig. S16), i.e., a mixture identical to that obtained by saturating a solution of host **1** with guest **2**, confirming that $\mathbf{2}_2 \subset \mathbf{1}$ is only stable in the presence of excess of free **1**. In addition to X-ray crystallography, the identity of $\mathbf{2}_2 \subset \mathbf{1}$ was confirmed using ^{13}C NMR and several 2D NMR techniques, including ^{1}H diffusion-ordered spectroscopy (DOSY), ^{1}H-^{1}H homonuclear correlation spectroscopy (COSY), ^{1}H-^{1}H nuclear Overhauser effect spectroscopy (NOESY), and ^{1}H-^{13}C heteronuclear single quantum correlation spectroscopy (HSQC) (*SI Appendix*, Figs. S6–S11).

A single set of well-defined signals observed for **2** (*SI Appendix*, Fig. S5) implies that the final mixture comprises ∼60% of $\mathbf{2}_2 \subset \mathbf{1}$ and ∼40% of empty **1** (i.e., no 1:1 complex **2** ⊂ **1** is formed). The fact that only a fraction of cage molecules becomes filled during stirring with an excess of **2** can be explained by the low solubility of free **2** in pure water (6.4 mg/L). Given that the concentration of the saturated solution of **2**, $c = 3.5 \cdot 10^{-5}$ M and that the equilibrium molar ratio $[\mathbf{2}_2 \subset \mathbf{1}]/[\mathbf{1}]$ corresponds to ∼1.5, it becomes possible to roughly estimate the association constant, $K_a = [\mathbf{2}_2 \subset \mathbf{1}]/[\mathbf{1}]\cdot[\mathbf{2}]^2$, as $\sim 10^9$ M^{-2} (or, assuming that a dimer of **2** is bound as a single species, $\sim 10^5$ M^{-1}). These values are similar to values previously determined for various inclusion complexes in aqueous media (35–39).

To gain further insight into the interactions between **1** and **2**, we recorded a series of ^{1}H NMR spectra of **1** in the presence of increasing amounts of the guest (*SI Appendix*, Fig. S12). Interestingly, we found that the presence of **2** caused a significant broadening of the signal due to **1**'s C_2 imidazole protons (H_a in *SI Appendix*, Fig. S13). Signal broadening can be understood by the coexistence of two rapidly interconverting forms of the host (i.e., guest-free **1** and $\mathbf{2}_2 \subset \mathbf{1}$) as a result of a rapid (on the NMR scale) exchange of guests between the hosts. Indeed, comparison of the X-ray structure of guest-free **1** (33) with that of $\mathbf{2}_2 \subset \mathbf{1}$ revealed that upon encapsulation of $\mathbf{2}_2$, the cage undergoes a significant conformational change, which is best manifested by the C_2–C_2 distance decreasing markedly from 4.01 to 3.51 Å (and the corresponding H_a–H_a distance, from 3.68 to 2.98 Å). Similarly, appreciable peak broadening was observed for **1**'s C_5 imidazole protons (H_b in *SI Appendix*, Fig. S13), which can be rationalized by these atoms pointing toward the interior of the cage and therefore interacting with the bound guest.

We hypothesized that this structural flexibility of **1** could be the key to accommodating both *trans* and *cis* isomers of the same azobenzene, thus providing a nanoenvironment suitable for efficiently switching these molecules. We were pleased to find that exposing an aqueous solution of $\mathbf{2}_2 \subset \mathbf{1}$ to a 365-nm (UV) light-emitting diode (LED) radiation source resulted in a major decrease in the main absorption peak and a concomitant increase in the less intense band at ∼420 nm (which can be attributed to the $n \rightarrow \pi^*$ transition of *cis*-azobenzene; Fig. 1*E*). However, analysis of NMR spectra of the irradiated solutions showed that the amount of *cis*-**2** was limited to only ∼60% (e.g., Fig. 1*C*, spectrum *iii*), even after irradiating for long times or with a high-intensity, 100-W UV lamp. To explain the relatively low conversion efficiency, we note that azobenzene's *cis* isomer is significantly more bulky than is *trans* (27, 28, 40), and we therefore propose the following two-step mechanism. In the first step, photoisomerization of one of two bound guests takes place, giving rise to **1** encapsulating a heterodimer of *trans*- and *cis*-azobenzene:

$$(\textit{trans}\text{-}\mathbf{2})_2 \subset \mathbf{1} \rightarrow (\textit{trans}\text{-}\mathbf{2}\cdot\textit{cis}\text{-}\mathbf{2}) \subset \mathbf{1}.$$

The ternary complex (*trans*-**2**·*cis*-**2**) ⊂ **1** is stable and it was observed by ^{1}H-^{1}H NOESY NMR (*SI Appendix*, Fig. S21). Then, the second molecule of **2** isomerizes—provided the availability of free **1** capable of stabilizing the resulting *cis*-**2**,

$$(\textit{trans}\text{-}\mathbf{2}\cdot\textit{cis}\text{-}\mathbf{2}) \subset \mathbf{1} + \mathbf{1} \rightarrow \textit{cis}\text{-}\mathbf{2} \subset \mathbf{1} + \textit{cis}\text{-}\mathbf{2} \subset \mathbf{1}.$$

To confirm this reasoning, we diluted the solution of **1** saturated with **2** (i.e., 60% $\mathbf{2}_2 \subset \mathbf{1}$ and 40% **1**) with one extra equivalent of **1**

and found that the photoisomerization efficiency increased to 72%. Upon treating the resulting solution with an additional two equivalents of **1**, the yield of *cis*-**2** increased further to 85%.

Upon subsequent exposure to blue light, the *trans* isomer of **2** was largely regenerated, and a photostationary state comprising 89% *trans*-**2** and 11% of residual *cis* was established (Fig. 1*C*, spectrum *iv*, and Fig. 1*E*, blue trace). The system could be switched between the UV- and blue-adapted states for multiple cycles without any appreciable fatigue (*SI Appendix*, Fig. S17).

The above mechanism of azobenzene isomerization/trafficking between cages is supported by more detailed studies in which we investigated the photoisomerization of azobenzene within $\mathbf{2}_2 \subset \mathbf{1}$ using in situ irradiation (with an optical fiber inserted into the NMR spectrometer). *SI Appendix*, Figs. S18 and S19 show the changes in the ^{1}H NMR spectra of $\mathbf{2}_2 \subset \mathbf{1}$ during (*i*) UV and (*ii*) blue light irradiation, where the peaks resonating at 6.19 and 6.72 ppm originate from the *ortho* and *meta* protons of *trans*-**2**, respectively. In (*i*), the peaks gradually shift to 6.07 and 6.84 ppm, respectively, which can be attributed to *trans*-**2** within (*trans*-**2**·*cis*-**2**) ⊂ **1**. This shift—as opposed to the emergence of new peaks at the expense of the original ones—can be explained by the rapid exchange of guests between filled and empty cages. In (*ii*), however, the cages are filled with either *cis*-**2** or *trans*-**2**/*cis*-**2** heterodimer; therefore, no fast guest exchange is possible. As a result, two well-defined sets of signals—due to (*trans*-**2**·*cis*-**2**) ⊂ **1** and $(\textit{trans}\text{-}\mathbf{2})_2 \subset \mathbf{1}$—could be seen. Notably, the final spectrum shows the residual *cis*-**2**, but no *trans*-**2**/*cis*-**2** heterodimer (*SI Appendix*, Fig. S18, *Top* spectrum), indicating that the back-isomerization reaction takes place more readily in (*trans*-**2**·*cis*-**2**) ⊂ **1** compared with *cis*-**2** ⊂ **1**.

Inspection of the X-ray structure of $(\textit{trans}\text{-}\mathbf{2})_2 \subset \mathbf{1}$ led us to hypothesize that **1**'s capacity to encapsulate azobenzenes should not be affected by placing additional substituents at their *para*-positions. To verify this hypothesis, we worked with 4-allyloxyazobenzene **3** (41) as a model *para*-substituted azobenzene and found that indeed it could be readily solubilized in aqueous solutions of the cage. Similar to $\mathbf{2}_2 \subset \mathbf{1}$, inclusion complex $\mathbf{3}_2 \subset \mathbf{1}$ was comprehensively characterized by a combination of 1D and 2D NMR techniques (*SI Appendix*, Figs. S23–S29). Integrating **1** and **3**'s signals in the ^{1}H NMR spectra revealed that the complex was formed in ∼35% yield, with ∼65% of the cages remaining empty, which can be rationalized by the extremely low solubility of **3** in pure water. An X-ray crystal structure of $\mathbf{3}_2 \subset \mathbf{1}$ confirmed that the *para*-substituents protruded outward (*SI Appendix*, Fig. S30) and could potentially be replaced by other functional groups. Remarkably, UV irradiation of $(\textit{trans}\text{-}\mathbf{3})_2 \subset \mathbf{1}$ led to a near-quantitative formation of the *cis* isomer (no residual *trans* could be detected by NMR spectroscopy, see *SI Appendix*, Fig. S34), which could be attributed to a large excess of empty **1**, capable of accommodating *cis*-**3**. *Cis* → *trans* back-isomerization proceeded upon exposure to blue light (*SI Appendix*, Fig. S35*A*) and the reaction could be repeated for multiple cycles (*SI Appendix*, Fig. S35*B*). Importantly, these results pave the way toward using **1** as a "supramolecular handcuff" (42) for constructing novel light-responsive systems.

Encouraged by these results, we considered encapsulating and studying the photoswitching of another structurally simple azobenzene, namely, tetra-*o*-methoxyazobenzene (**4** in Fig. 2*A*). An attractive feature of *ortho*-substituted azobenzenes is that their *trans* isomers' absorption bands extend far into the visible region and that they can be efficiently isomerized using yellow or even red light (43–45) (we worked with a 580-nm LED). Moreover, their *cis* isomers typically have long thermal half-lives; in fact, by following the previously published literature procedure (45), we obtained **4** as a ∼9:1 mixture of *cis* and *trans* isomers. Incubating this mixture with an aqueous solution of **1** afforded an inclusion complex containing exclusively *cis*-**4** as the guest (Fig. 2*B*, *Top* spectrum; see also *SI Appendix*, Figs. S36–S42), indicating that **1** has a higher affinity for the *cis* isomer of **4**. A single set of sharp signals for the acidic imidazole protons (in the 9.3–8.7 ppm range) indicates that practically all of the cages become filled.

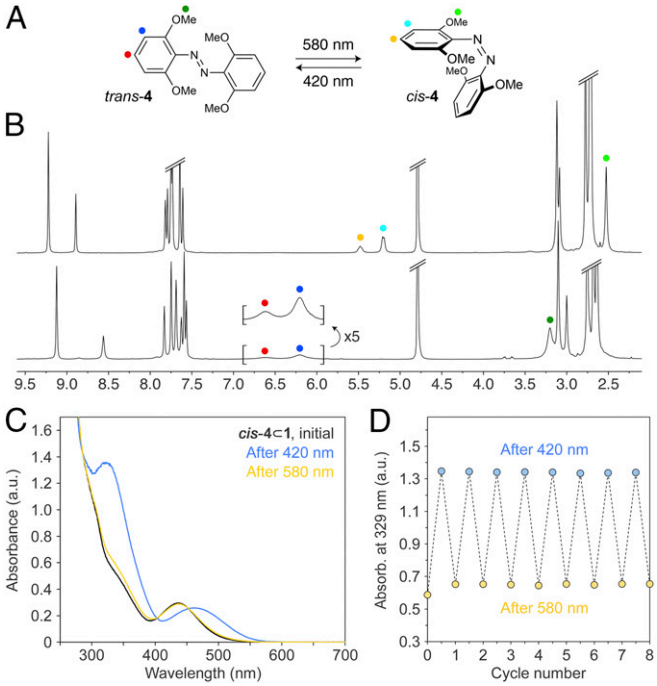

Fig. 2. Reversible photoswitching of tetra-*o*-methoxyazobenzene **4** in water. (*A*) Yellow/blue light-induced isomerization of **4**. (*B*) The ^{1}H NMR spectra of inclusion complex **4** ⊂ **1** obtained by encapsulating *cis*-**4** (*Upper*) and *trans*-**4** (*Lower*) (500 MHz, D_2O, 298 K). (*C*) Changes in the UV/Vis absorption spectrum of *cis*-**4** ⊂ **1** following exposure to blue light (5 min) and then to yellow light (90 min). (*D*) Eight cycles of reversible photoisomerization of **4** within **4** ⊂ **1**, followed by UV/Vis absorption spectroscopy.

We separately studied the complexation of pure *trans*-**4** (obtained by irradiating the *cis* isomer with blue light) and similarly found that an inclusion complex was formed in a ∼100% yield (Fig. 2*B*, *Bottom* spectrum; see also *SI Appendix*, Fig. S44). Interestingly, both complexes were of 1:1 stoichiometry, which most likely is due to the bulky nature of **4** associated with the four methoxy groups. Another indication of a different mode of binding is provided by experiments in which we monitored the encapsulation kinetics by UV/Vis spectroscopy and found (*SI Appendix*, Fig. S4) that both isomers of **4** were encapsulated markedly slower than were azobenzenes forming 2:1 complexes (where the binding of one guest could facilitate the encapsulation of another). Unfortunately, despite extensive efforts, we did not succeed in obtaining single crystals of either isomer of **4** ⊂ **1** of a quality suitable for X-ray diffraction studies.

Reversible isomerization between *trans*-**4** ⊂ **1** and *cis*-**4** ⊂ **1** was achieved by alternately irradiating the solution with yellow and blue light (Fig. 2 *C* and *D*). Notably, excellent photostationary states were observed, with the blue-adapted and the yellow-adapted states comprising ∼93% *trans* and ∼100% *cis*, respectively (*SI Appendix*, Figs. S43 and S47). By stopping the irradiation before the reaction was completed, we isolated mixtures containing roughly equal amounts of both isomers of **4**. We analyzed these samples by ^{1}H-^{1}H NOESY NMR spectra (e.g., *SI Appendix*, Fig. S49) and found no evidence of nuclear Overhauser (nOe) correlations between *trans*- and *cis*-**4**, suggesting that they cannot coexist within the same cage molecule. These results further confirm the 1:1 stoichiometry of inclusion complex **4** ⊂ **1**.

Finally, we considered another red-shifted derivative—tetra-*o*-fluoroazobenzene **5** (46)—as a potential guest for **1**. *Trans*-**5** can be conveniently isomerized to its *cis* form using green (520 nm) light (47), with the back-isomerization reaction occurring under blue (420 nm) irradiation (Fig. 3*A*). We found that similar to its

nonfluorinated counterpart, **2**, azobenzene **5** formed a 2:1 inclusion complex with **1** (i.e., $\mathbf{5}_2 \subset \mathbf{1}$), whose X-ray structure and NMR spectrum are shown in Fig. 3 *B* and *C* (top spectrum), respectively. Interestingly, **5** within $\mathbf{5}_2 \subset \mathbf{1}$ retained its photoswitchable properties: exposing it to green light significantly decreased the absorption in the UV region, whereas subsequent irradiation with blue light restored the original spectrum (Fig. 3 *D* and *E*), indicating a high reversibility of photoswitching. However, we also found some notable differences between **5** and **2**. First, inclusion complex $\mathbf{5}_2 \subset \mathbf{1}$ was formed in a quantitative yield (i.e., practically all of the cages could be filled with a dimer of **5**). Second, NMR spectra of **1** recorded in the presence of a substoichiometric (i.e., <2 eq) amount of guest **5** showed the presence of two pairs of imidazole signals: one corresponding to filled, and the other to empty **1** (highlighted in green and red, respectively, in Fig. 3*C*). The presence of distinct signals for free and filled cages indicates a relatively slow (on the NMR scale) exchange of the guests between the cages. Importantly, the relative intensities of these signals confirmed that **5** is encapsulated as a dimer: for example, mixing **1** and **5** in a 1:1 molar ratio afforded a spectrum (blue in Fig. 3*C*), in which the signals due to filled and empty **1** had the same intensity. Third, exposure of relatively concentrated (millimole range) solutions of $\mathbf{5}_2 \subset \mathbf{1}$ to green light resulted in a precipitation reaction (*SI Appendix*, Fig. S65). The resulting yellow, crystalline precipitate was stable until irradiated with blue light, which regenerated the original solution of (*trans*-**5**)$_2 \subset$ **1**. The light-induced precipitation-dissolution sequence could be repeated for many cycles.

We analyzed the yellow crystals by ^{1}H NMR (*SI Appendix*, Fig. S66) and X-ray diffraction, and found that they were composed of pure *cis*-**5**, suggesting that, unlike heterodimer *trans*-**2**·*cis*-**2** (see above), *trans*-**5**·*cis*-**5** is not stable within the same cage molecule—in other words, *trans* → *cis* isomerization entails the removal of one of two guests from the cage (Fig. 3*F*), a scenario supported by the following observations. First, we exposed a solution of (*trans*-**5**)$_2 \subset$ **1** to green light and collected the supernatant by centrifugation. We then compared the UV/Vis absorption spectrum of the supernatant (*cis*-**5** $\subset$ **1**) to the spectrum of a solution of the precipitate (i.e., *cis*-**5**) in the same volume of an organic solvent. These two spectra were nearly overlapping (*SI Appendix*, Fig. S67), indicating that ∼50% of **5** contained within (*trans*-**5**)$_2 \subset$ **1** was expelled from the cage (for additional evidence, see *SI Appendix*, Fig. S67). Second, we compared the ^{1}H NMR spectrum of (*trans*-**5**)$_2 \subset$ **1** before and after exposure to green light (followed by discarding the precipitate) and concluded that the **5**:**1** molar ratio decreased from ∼2 to ∼1 (*SI Appendix*, Fig. S68). Notably, no precipitation was observed in the second cycle, i.e., after "resetting" the system with blue light followed by shining green light. This result can be understood by taking into consideration the presence of 1 eq of free cage, which can accommodate the *cis*-**5** originally expelled from (*trans*-**5**)$_2 \subset$ **1**, according to the reaction equation,

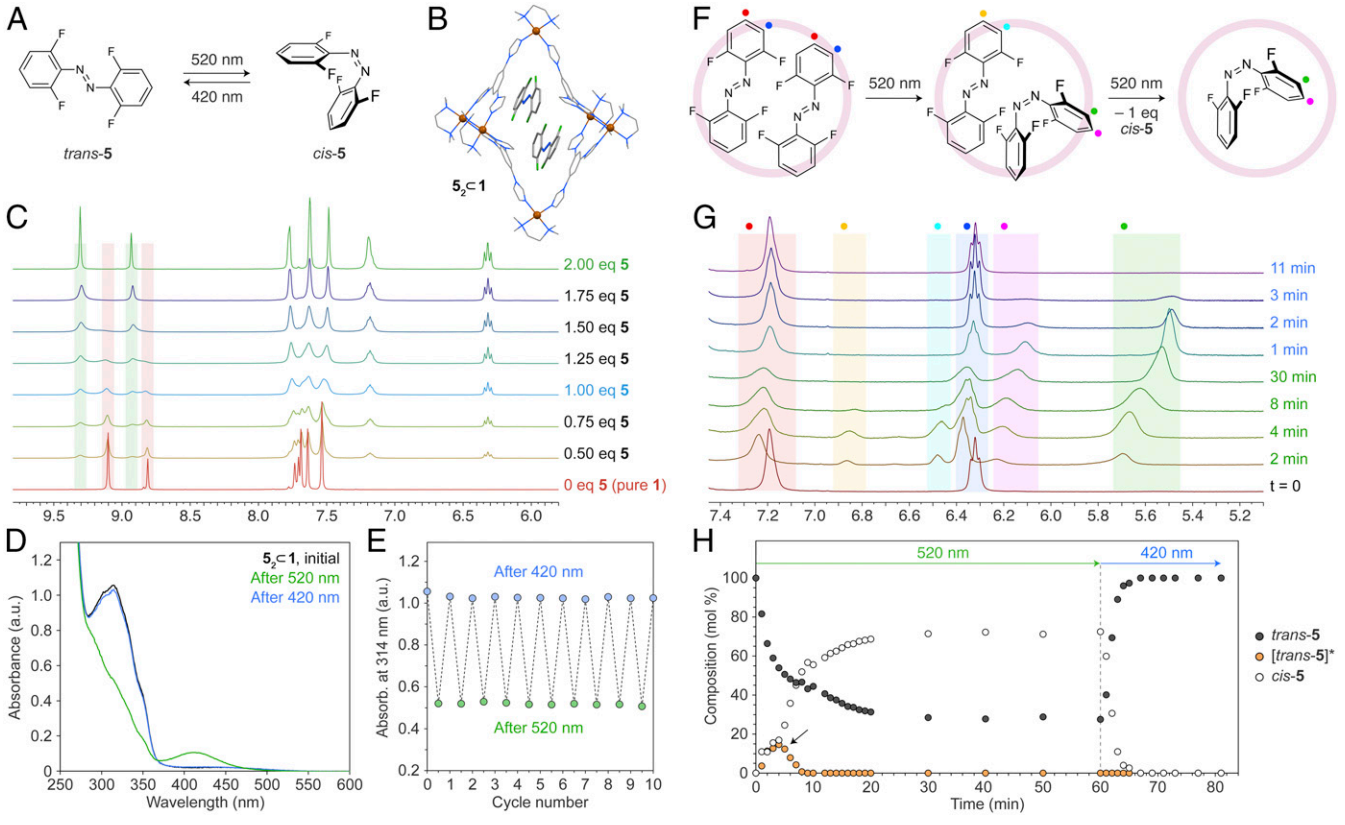

Fig. 3. Reversible photoswitching of tetra-*o*-fluoroazobenzene **5** in water. (*A*) Green/blue light-induced isomerization of **5**. (*B*) X-ray crystal structure of (*trans*-**5**)$_2 \subset$ **1** (see also *SI Appendix*, Fig. S60). (*C*) Partial ^{1}H NMR spectra of cage **1** in the presence of increasing amounts of guest **5** (500 MHz, D_2O, 298 K). The signals highlighted in red correspond to imidazole (N=C**H**–N) protons of empty **1** and those highlighted in green correspond to **1** filled with 2 eq of **5**. (*D*) Changes in the UV/Vis absorption spectrum of (*trans*-**5**)$_2 \subset$ **1** following exposure to green light (4 min) and then to blue light (4 min). (*E*) Ten cycles of reversible photoisomerization of **5** within $\mathbf{5}_2 \subset$ **1**, followed by UV/Vis absorption spectroscopy. (*F*) The stepwise mechanism underlying the *trans* → *cis* photoisomerization of $\mathbf{5}_2 \subset$ **1**. (*G*) Changes in ^{1}H NMR spectra of (*trans*-**5**)$_2 \subset$ **1** (bottom spectrum) during irradiation with 520-nm light (indicated in green font) for up to 30 min and subsequently with 420-nm light (blue font) for up to 11 min (500 MHz, D_2O, 298 K). For a complete set of spectra, please refer to *SI Appendix*, Fig. S62. (*H*) Changes in the relative concentrations of different isomers of **5** as a function of irradiation. White markers denote encapsulated *cis*-**5**; black markers denote *trans*-**5** within (*trans*-**5**)$_2 \subset$ **1**; orange markers denote *trans*-**5** within (*trans*-**5**·*cis*-**5**) $\subset$ **1**. The peak indicated with an arrow is due to transient intermediate (*trans*-**5**·*cis*-**5**) $\subset$ **1**.

$$(trans\text{-}\mathbf{5})_2 \subset \mathbf{1} + \mathbf{1} \rightarrow cis\text{-}\mathbf{5} \subset 1 + cis\text{-}\mathbf{5} \subset \mathbf{1}.$$

To obtain further insight into the photoisomerization of (*trans*-**5**)$_2$ ⊂ **1**, we studied it with in situ NMR spectroscopy. The series of spectra shown in *SI Appendix*, Fig. S62 (see also the analysis in Fig. 3*H*) revealed that the reaction proceeded in three stages. First (0–4 min), we observed the emergence of two new sets of peaks, which can be attributed to *trans*-**5** (highlighted in yellow and cyan in Fig. 3*G*) and *cis*-**5** (pink and green) within the metastable (*trans*-**5**·*cis*-**5**) ⊂ **1** ternary complex:

$$(trans\text{-}\mathbf{5})_2 \subset \mathbf{1} \rightarrow (trans\text{-}\mathbf{5} \cdot cis\text{-}\mathbf{5}) \subset \mathbf{1}.$$

Once the molar fraction of the ternary complex reached ∼30%, the concentration of *cis*-**5** increased sharply (4–8 min in Fig. 3*H*), suggesting the expulsion of the preformed *cis*-**5** concomitant with a rapid isomerization of the remaining guest:

$$(trans\text{-}\mathbf{5} \cdot cis\text{-}\mathbf{5}) \subset \mathbf{1} \rightarrow cis\text{-}\mathbf{5} \subset \mathbf{1} + cis\text{-}\mathbf{5}\downarrow.$$

Importantly, these results support our view that the photoswitching reaction occurred inside the cage. Indeed, the (*trans*-**5**·*cis*-**5**) ⊂ **1** species was not observed upon mixing preformed (*trans*-**5**)$_2$ ⊂ **1** and *cis*-**5** ⊂ **1** (concluded from the ^{1}H and ^{1}H-^{1}H NOESY spectra; *SI Appendix*, Fig. S58).

In the third stage of the process (8–30 min), the *trans* → *cis* isomerization continued, but without the involvement of the transient ternary complex,

$$(trans\text{-}\mathbf{5})_2 \subset \mathbf{1} \rightarrow cis\text{-}\mathbf{5} \subset \mathbf{1} + cis\text{-}\mathbf{5}\downarrow.$$

suggesting that the photoisomerization was facilitated by the presence of preexisting seeds of *cis*-**5**. Once a photostationary state was reached, exposure to blue light rapidly converted the *cis*-**5** ⊂ **1** + *cis*-**5**↓ mixture directly into the initial (*trans*-**5**)$_2$ ⊂ **1** inclusion complex (Fig. 3 *G* and *H*).

The large change in the solution's opacity induced by green light (*SI Appendix*, Fig. S65) inspired us to consider fabricating an information storage medium, in which messages could be written and erased using two different wavelengths of light. To this end, we first investigated light-induced crystallization in thin films of agarose-based hydrogels soaked in an aqueous solution of **5**$_2$ ⊂ **1**. First, the rectangular piece of gel shown in Fig. 4*A* was exposed to 520-nm LED light for increasing periods of time. Ten seconds of irradiation had little effect on the film, which remained transparent. However, exposure to 20 s of light resulted in the formation of millimeter-long, needlelike crystals of *cis*-**5** at a density of ∼2 per mm^2. Extending the irradiation time increased the density of the crystals, whereas their sizes decreased, indicating a larger number of nucleation events. Gels exposed to 2 min of green light became densely doped with microcrystals, which acted as efficient light scatterers and prevented stray light from passing through the film (Fig. 4*A*). The resulting opaque film was stable: no appreciable changes were found after 30 d in the dark. Remarkably, however, exposure to 5 min of blue light caused the crystals to disappear [*cis*-**5**↓ + *cis*-**5** ⊂ **1** → (*trans*-**5**)$_2$ ⊂ **1**], and the original transparent film was regenerated.

Next, we hypothesized that exposing these **5**$_2$ ⊂ **1**-soaked gels to green light locally (e.g., through a mask; Fig. 4*B*) could result in high-contrast, high-resolution patterns. Fig. 4*C*, *Top Left*, shows an example of one such pattern created by exposing a millimeter-thick, 5 × 4 cm piece of gel to 5 min of green light. Subsequent irradiation with blue light (5 min) was used to "erase" the image, and the cycle could be repeated. Multiple images could be created consecutively in the same piece of hydrogel without any apparent fatigue (Fig. 4*C*). It is worth recalling that numerous examples of reversible information storage media based on photochromic dyes [mainly diarylethenes (48), spiropyrans (49), and spirooxazines (50)] have been reported. Although based on a photochromic dye, our system is unique in that the high contrast originates from different degrees of light scattering rather than from different light absorption properties. Our system is also conceptually different from the recently developed information storage media based on reversible self-assembly on plasmonic nanoparticles (51, 52). Whereas patterns created in these media persisted only for defined periods (varying between seconds and days), our system is bistable in that applying a competing stimulus (here, blue light) is necessary to erase the information.

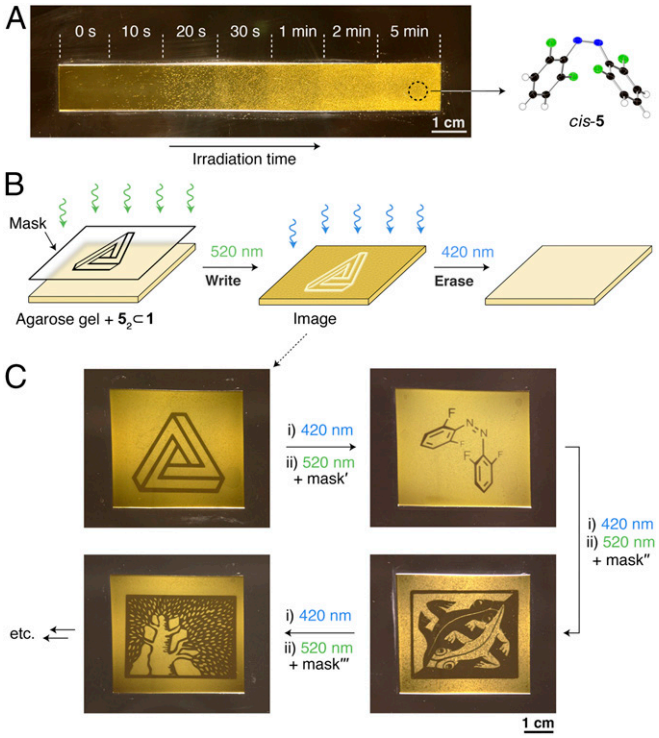

Fig. 4. Light-induced expulsion of fluorinated azobenzene **5** from coordination cage **1**. (*A*) Thin piece of agarose gel soaked with an aqueous solution of (*trans*-**5**)$_2$ ⊂ **1** subjected to 520-nm irradiation for increasing periods of time (indicated on the top). (*Right*) X-ray crystal structure of *cis*-**5**. (*B*) Writing and erasing an image in a **5**$_2$ ⊂ **1**-soaked agarose gel using green light (with a mask) and blue light, respectively. (*C*) Four images created consecutively in the same piece of light-sensitive agarose gel. Clockwise from *Top Left*: the Penrose triangle, the structural formula of *cis*-**5**, *Plane-Filling Motif with Reptiles* (a 1941 woodcut by M. C. Escher; all M.C. Escher works © 2018 The M.C. Escher Company, The Netherlands. All rights reserved. Used by permission. www.mcescher.com), and part of the logo of the Weizmann Institute (reproduced with permission of the Weizmann Institute of Science).

Finally, we were interested in whether the encapsulated azobenzenes retain their photoswitchable properties in the solid state. Thin polycrystalline films of **2**$_2$ ⊂ **1** and **5**$_2$ ⊂ **1** on glass slides were prepared by slow evaporation of water from the respective solutions. Interestingly, irradiating these samples with UV and green light, respectively, resulted in an increase in absorbance at ∼420 nm (due to the n → π* transition in *cis*-azobenzene), which was particularly pronounced for **5**$_2$ ⊂ **1** (*SI Appendix*, Fig. S71). Following exposure to blue light, the ∼420 nm band decreased to the original level and the process could be repeated for multiple cycles. Notably, no changes in the UV/Vis spectra of nonencapsulated crystalline **2** or **5** could be detected upon exposure to UV or green light, confirming the critical role of the host in facilitating the photoisomerization process. Our results are reminiscent of those obtained by Credi and coworkers (53) who observed solid-state photoisomerization of azobenzene within thin films of porous molecular crystals.

In sum, we investigated the encapsulation and photoinduced isomerization of several azobenzenes within a self-assembled

coordination cage. Depending on the substitution pattern on the azobenzene core, inclusion complexes containing one or two guest molecules were formed. The binding of azobenzenes was accompanied by a pronounced change in the conformation of the cage. This conformational flexibility was also important for the successful photoisomerization of the encapsulated azobenzenes as demonstrated by NMR studies. Isomerization of a fluorinated azobenzene was accompanied by its expulsion from the cage—a finding that was used to fabricate a reversible information storage medium. Future research should focus on encapsulating other photochromic molecules (such as arylazopyrazoles and diarylethenes) and investigating their properties under confinement. At the same time, flexible cages featuring expanded cavities will be synthesized with the goal of encapsulating higher oligomers of azobenzene—here, we are particularly interested in systematically studying cooperative switching processes (54–56). Finally, our results indicate that light energy can be used (via the noncovalently bound molecular switch) to reversibly change the shape of a nonphotoresponsive molecular system (here, a self-assembled cage), thus paving the way toward the development of novel artificial molecular machines.

ACKNOWLEDGMENTS. We gratefully acknowledge Dr. Liat Avram for helpful discussions. This work was supported by the European Research Council (Grant 336080).

1. Muraoka T, Kinbara K, Aida T (2006) Mechanical twisting of a guest by a photoresponsive host. *Nature* 440:512–515.
2. Ragazzon G, Baroncini M, Silvi S, Venturi M, Credi A (2015) Light-powered autonomous and directional molecular motion of a dissipative self-assembling system. *Nat Nanotechnol* 10:70–75.
3. Štacko P, et al. (2017) Locked synchronous rotor motion in a molecular motor. *Science* 356:964–968.
4. Fletcher SP, Dumur F, Pollard MM, Feringa BL (2005) A reversible, unidirectional molecular rotary motor driven by chemical energy. *Science* 310:80–82.
5. Cheng C, et al. (2015) An artificial molecular pump. *Nat Nanotechnol* 10:547–553.
6. Wilson MR, et al. (2016) An autonomous chemically fuelled small-molecule motor. *Nature* 534:235–240.
7. Collins BSL, Kistemaker JCM, Otten E, Feringa BL (2016) A chemically powered unidirectional rotary molecular motor based on a palladium redox cycle. *Nat Chem* 8:860–866.
8. Sauvage J-P (2017) From chemical topology to molecular machines (Nobel Lecture). *Angew Chem Int Ed Engl* 56:11080–11093.
9. Stoddart JF (2017) Mechanically interlocked molecules (MIMs)—Molecular shuttles, switches, and machines (Nobel Lecture). *Angew Chem Int Ed Engl* 56:11094–11125.
10. Feringa BL (2017) The art of building small: From molecular switches to motors (Nobel Lecture). *Angew Chem Int Ed Engl* 56:11060–11078.
11. Lewandowski B, et al. (2013) Sequence-specific peptide synthesis by an artificial small-molecule machine. *Science* 339:189–193.
12. Kassem S, et al. (2017) Stereodivergent synthesis with a programmable molecular machine. *Nature* 549:374–378.
13. Katsonis N, Lubomska M, Pollard MM, Feringa BL, Rudolf P (2007) Synthetic light-activated molecular switches and motors on surfaces. *Prog Surf Sci* 82:407–434.
14. Zhang Q, Qu DH (2016) Artificial molecular machine immobilized surfaces: A new platform to construct functional materials. *ChemPhysChem* 17:1759–1768.
15. Nguyen TD, et al. (2005) A reversible molecular valve. *Proc Natl Acad Sci USA* 102: 10029–10034.
16. Klajn R, Stoddart JF, Grzybowski BA (2010) Nanoparticles functionalised with reversible molecular and supramolecular switches. *Chem Soc Rev* 39:2203–2237.
17. Li Z, Barnes JC, Bosoy A, Stoddart JF, Zink JI (2012) Mesoporous silica nanoparticles in biomedical applications. *Chem Soc Rev* 41:2590–2605.
18. Bernà J, et al. (2005) Macroscopic transport by synthetic molecular machines. *Nat Mater* 4:704–710.
19. Liu Y, et al. (2005) Linear artificial molecular muscles. *J Am Chem Soc* 127:9745–9759.
20. Wang R, et al. (1997) Structural investigation of azobenzene-containing self-assembled monolayer films. *J Electroanal Chem (Lausanne)* 438:213–219.
21. Kusukawa T, Fujita M (1999) "Ship-in-a-bottle" formation of stable hydrophobic dimers of *cis*-azobenzene and -stilbene derivatives in a self-assembled coordination nanocage. *J Am Chem Soc* 121:1397–1398.
22. Clever GH, Tashiro S, Shionoya M (2010) Light-triggered crystallization of a molecular host-guest complex. *J Am Chem Soc* 132:9973–9975.
23. Dube H, Ajami D, Rebek J, Jr (2010) Photochemical control of reversible encapsulation. *Angew Chem Int Ed Engl* 49:3192–3195.
24. del Barrio J, et al. (2013) Photocontrol over cucurbit[8]uril complexes: Stoichiometry and supramolecular polymers. *J Am Chem Soc* 135:11760–11763.
25. Yamaguchi H, et al. (2012) Photoswitchable gel assembly based on molecular recognition. *Nat Commun* 3:603.
26. Nalluri SKM, Ravoo BJ (2010) Light-responsive molecular recognition and adhesion of vesicles. *Angew Chem Int Ed Engl* 49:5371–5374.
27. Brown CJ (1966) A refinement of the crystal structure of azobenzene. *Acta Crystallogr* 21:146–152.
28. Mostad A, Rømming C (1971) A refinement of the crystal structure of *cis*-azobenzene. *Acta Chem Scand* 25:3561–3568.
29. Yoshizawa M, Klosterman JK, Fujita M (2009) Functional molecular flasks: New properties and reactions within discrete, self-assembled hosts. *Angew Chem Int Ed Engl* 48:3418–3438.
30. Liu Z, Nalluri SKM, Stoddart JF (2017) Surveying macrocyclic chemistry: From flexible crown ethers to rigid cyclophanes. *Chem Soc Rev* 46:2459–2478.
31. Rizzuto FJ, Nitschke JR (2017) Stereochemical plasticity modulates cooperative binding in a $Co^{II}_{12}L_6$cuboctahedron. *Nat Chem* 9:903–908.
32. Mondal P, Sarkar S, Rath SP (2017) Cyclic bis-porphyrin-based flexible molecular containers: Controlling guest arrangements and supramolecular catalysis by tuning cavity size. *Chemistry* 23:7093–7103.
33. Samanta D, et al. (2018) Reversible chromism of spiropyran in the cavity of a flexible coordination cage. *Nat Commun* 9:641.
34. Samanta D, Mukherjee S, Patil YP, Mukherjee PS (2012) Self-assembled Pd_6 open cage with triimidazole walls and the use of its confined nanospace for catalytic Knoevenagel- and Diels-Alder reactions in aqueous medium. *Chemistry* 18:12322–12329.
35. Zhao N, Liu L, Biedermann F, Scherman OA (2010) Binding studies on CB[6] with a series of 1-alkyl-3-methylimidazolium ionic liquids in an aqueous system. *Chem Asian J* 5:530–537.
36. Slone RV, Hupp JT (1997) Synthesis, characterization, and preliminary host-guest binding studies of porphyrinic molecular squares featuring *fac*-tricarbonylrhenium(I) chloro corners. *Inorg Chem* 36:5422–5423.
37. Sun H, Gibb CLD, Gibb BC (2008) Calorimetric analysis of the 1:1 complexes formed between a water-soluble deep-cavity cavitand, and cyclic and acyclic carboxylic acids. *Supramol Chem* 20:141–147.
38. Piatnitski EL, Flowers RA, 2nd, Deshayes K (2000) Highly organized spherical hosts that bind organic guests in aqueous solution with micromolar affinity: Microcalorimetry studies. *Chemistry* 6:999–1006.
39. Cullen W, Turega S, Hunter CA, Ward MD (2015) Virtual screening for high affinity guests for synthetic supramolecular receptors. *Chem Sci* 6:2790–2794.
40. Döbbelin M, et al. (2016) Light-enhanced liquid-phase exfoliation and current photoswitching in graphene-azobenzene composites. *Nat Commun* 7:11090.
41. Ledin PA, et al. (2014) Star-shaped molecules with polyhedral oligomeric silsesquioxane core and azobenzene dye arms. *Langmuir* 30:8856–8865.
42. Rauwald U, Scherman OA (2008) Supramolecular block copolymers with cucurbit[8]uril in water. *Angew Chem Int Ed Engl* 47:3950–3953.
43. Wheeler OH, Gonzalez D (1964) Oxidation of primary aromatic amines with manganese dioxide. *Tetrahedron* 20:189–193.
44. Samanta S, et al. (2013) Photoswitching azo compounds in vivo with red light. *J Am Chem Soc* 135:9777–9784.
45. Hansen MJ, Lerch MM, Szymanski W, Feringa BL (2016) Direct and versatile synthesis of red-shifted azobenzenes. *Angew Chem Int Ed Engl* 55:13514–13518.
46. Sugawara S, Ishikawa N, Harada H, Hayashi S (1973) Synthesis of fluorinated aromatic monomers. VII. Preparation of sym-polyfluorodiaminobiphenyls. *Nippon Kagaku Kaishi* 8:1510–1514.
47. Bléger D, Schwarz J, Brouwer AM, Hecht S (2012) o-Fluoroazobenzenes as readily synthesized photoswitches offering nearly quantitative two-way isomerization with visible light. *J Am Chem Soc* 134:20597–20600.
48. Kobatake S, Yamashita I (2008) Synthesis of photochromic diarylethene polymers for a write-by-light/erase-by-heat recording system. *Tetrahedron* 64:7611–7618.
49. Jung Y, Lee H, Park TJ, Kim S, Kwon S (2015) Programmable gradational micropatterning of functional materials using maskless lithography controlling absorption. *Sci Rep* 5:15629.
50. Pardo R, Zayat M, Levy D (2009) Reaching bistability in a photochromic spirooxazine embedded sol-gel hybrid coatings. *J Mater Chem* 19:6756–6760.
51. Klajn R, Wesson PJ, Bishop KJM, Grzybowski BA (2009) Writing self-erasing images using metastable nanoparticle "inks". *Angew Chem Int Ed Engl* 48:7035–7039.
52. Kundu PK, et al. (2015) Light-controlled self-assembly of non-photoresponsive nanoparticles. *Nat Chem* 7:646–652.
53. Baroncini M, et al. (2015) Photoinduced reversible switching of porosity in molecular crystals based on star-shaped azobenzene tetramers. *Nat Chem* 7:634–640.
54. Pace G, et al. (2007) Cooperative light-induced molecular movements of highly ordered azobenzene self-assembled monolayers. *Proc Natl Acad Sci USA* 104: 9937–9942.
55. Moldt T, et al. (2015) Tailoring the properties of surface-immobilized azobenzenes by monolayer dilution and surface curvature. *Langmuir* 31:1048–1057.
56. Zheng YB, et al. (2013) Photoresponsive molecules in well-defined nanoscale environments. *Adv Mater* 25:302–312.